JOURNAL OF CATALYSIS 120, 325–336 (1989)

Physicochemical Properties of MoO_3–TiO_2 Prepared by an Equilibrium Adsorption Method

DU SOUNG KIM, YASUHIKO KURUSU, ISRAEL E. WACHS,*
FRANKLIN D. HARDCASTLE,* AND KOHICHI SEGAWA[1]

*Department of Chemistry, Faculty of Science and Technology, Sophia University, 7-1 Kioi-cho, Chiyoda-ku, Tokyo 102, Japan, and *Zettlemoyer Center for Surface Studies and Department of Chemical Engineering, Lehigh University, Bethlehem, Pennsylvania 18015*

Received February 28, 1989; revised July 12, 1989

The adsorption phenomena of molybdena species onto titania surfaces and the surface properties of the catalysts have been studied by using an equilibrium adsorption method. ^{95}Mo NMR and UV spectroscopic studies show that the aqueous molybdena species vary as a function of the pH of the impregnating solution. For acidic pH values, polymeric species, $Mo_7O_{24}^{6-}$ ions, are present, while in the basic solutions it is the monomeric MoO_4^{2-} ions that are present. The adsorbed amounts of molybdate anion are strongly dependent on the pH of the impregnating solution and increase as an inverse function of the pH. XRD, Raman, and XPS data of the calcined samples show that monolayer coverage of molybdenum oxide is established at pH 3.98 (6.6 wt%). The Raman studies reveal that the molybdenum oxide monolayer is composed of distorted octahedra. At more acidic pH regions, pH < 3.98, crystalline MoO_3 is formed above monolayer coverage. The results of catalytic oxidation of methanol show that the catalysts up to monolayer coverage of surface molybdate species possess higher turnover numbers than the catalysts possessing more than monolayer coverage (presence of crystalline MoO_3). The primary methanol oxidation product is dimethoxymethane at low conversions; methyl formate is next in abundance. The selectivity for dimethyl ether, which occurred as a side reaction on the acidic sites of catalysts, increases as the Mo loading increases.

INTRODUCTION

Molybdenum catalysts are widely used for hydrodesulfurization and hydrocracking of heavy fractions as well as for metathesis of alkenes in the petroleum industry. Recently, they were found to show catalytic activities for the partial oxidation of aliphatic alcohols (*1, 2*). The catalytic activity and selectivity are affected by the surface morphology. Allison and Goddard (*3*) proposed that the catalytic active site of methanol oxidation on MoO_3 catalyst involves two adjacent dioxo units (the dual dioxo units). Che *et al.* (*4*) have found that the selectivity of methanol oxidation is influenced not only by the environment of the Mo but also by the dispersion state of the molybdena species on the silica support. A number of studies on supported molybdena catalysts have been carried out to elucidate the structures of the molybdena catalysts which exert an effect on the catalytic activity (*5–8*). However, there are still debates about the structure of the molybdena species on the support and about their corresponding catalytic activities.

Supported molybdena catalysts have usually been prepared by coprecipitation or impregnation and/or incipient wetness methods. Recently, an equilibrium adsorption method was devised to overcome the drawbacks of these methods (*9–11*). In the equilibrium adsorption method, molybdate anions adsorb onto the positively charged titania surface via electrostatic attraction by controlling the pH of the impregnating solution. Therefore, the pH of the impregnating solution and the isoelectric point (IEP) of a support are essential parameters

[1] To whom all correspondence should be addressed.

0021-9517/89 $3.00

for regulating the surface properties of catalysts. Haight and Boston (*12*) pointed out that at high pH regions (pH > 6), MoO_4^{2-} ions are generally present in solution, but at acidic pH regions (1 < pH < 6) MoO_4^{2-} gives $Mo_7O_{24}^{6-}$ and $Mo_8O_{26}^{4-}$ ions. The hydroxyl groups of the titania surface in solution tend to be either positively or negatively charged below or above the IEP of titania (anatase: pH 6.2; rutile: pH 4.8–5.6) (*13, 14*):

$$Ti\text{–}OH_2^+ \leftrightharpoons Ti\text{–}OH \rightleftharpoons Ti\text{–}O^-. \quad (1)$$

The adsorbed amounts of molybdate anion are controlled by the number of positively charged hydroxyl groups on the titania surface. Above the IEP of titania, the hydroxyls of titania tend to be negatively charged, so that it is relatively hard for the molybdena species to be adsorbed on the titania surface, due to the electrostatic repulsion in the solution. D'Aniello (*15*) has reported that the adsorption process was reversible: desorption was brought out by adding a basic buffer.

The objectives of this study are (1) to elucidate the adsorption phenomena in the impregnating solution and (2) to determine the influence of the structure and corresponding surface properties of the adsorbed molybdena species on the catalytic activity of methanol oxidation.

EXPERIMENTAL

Catalyst preparation. Titania-supported molybdena catalysts were prepared by an equilibrium adsorption method (*9*). The materials employed in this study were P-25 titania from Degussa, with surface area of ca. 51 $m^2\ g^{-1}$, and analytical grade ammonium heptamolybdate. The titania support was composed of ca. 80% anatase and 20% rutile, as determined by XRD. Five grams of titania was impregnated at 323 K for 100 h with 0.007 *M* aqueous solution ammonium heptamolybdate. The pH of the impregnating solution was adjusted with HNO_3 or NH_4OH solution. The suspended solution was occasionally shaken in a thermostated bath. After adsorption, the solids were separated from the solution by filtration. All the wet catalysts were dried at 373 K for 24 h and then calcined in air at 773 K for 24 h. The adsorbed amounts of molybdenum as oxide base (wt% of MoO_3) were determined by chemical analysis (*16*).

^{95}Mo NMR and UV spectroscopy. The ^{95}Mo NMR spectra of 0.1 *M* Mo solution at different pH values were obtained at 17.4 MHz on a Fourier transform pulsed spectrometer (JEOL, JNM-GX270) using a 10-mm NMR sample tube. The chemical shifts were referenced to a 2 *M* aqueous solution of Na_2MoO_4. The UV spectra of the filtrates at different pH values were also measured after 100 h of equilibrium adsorption. The spectra (Shimadzu, UV-240) were obtained in the range from 190 to 500 nm.

XRD and X-ray photoelectron spectroscopy. X-ray powder diffraction (XRD) patterns of the calcined catalysts were obtained with a diffractometer (Rigaku Electronic, RAD-2A; Cu$K\alpha$, λ = 0.15405 nm). XPS measurements of the calcined catalysts were made on an XPS spectrometer (Surface Science Laboratory, SSX-100) with monochromatic Al$K\alpha$ radiation (1486.6 eV); charge compensation was effected by an electron floodgun.

Laser Raman spectroscopy. Laser Raman spectra of the calcined catalysts were obtained with an Instruments SA molecular optics laser examiner (MOLE) Raman microprobe. An Ar^+ ion laser (Spectra Physics, Model 164) delivered about 40 mW of incident radiation, and spectra were obtained by using the 514.5-nm excitation line. The spectral slit width was 5 cm^{-1}.

BET surface area and CO_2 chemisorption. Both experiments were performed with a standard BET adsorption system. BET surface areas of catalysts were determined by N_2 adsorption at 77 K. CO_2 adsorption isotherms of catalysts were measured at 293 K. Adsorption isotherms of the Langmuir type have been obtained for all catalysts. The CO_2 chemisorbed from each

catalyst was determined at the extrapolated pressure of zero.

Catalytic reactions. Oxidation of methanol was carried out at 473 K by using a closed recirculation system (157 cm^3) with a mixture of methanol and oxygen in the ratio of 1/3.4 (mole/mole). Ten milligrams of the catalysts was packed in the quartz tubular reactor. Prior to the reaction, the catalysts were treated with O_2 at 773 K for 3 h and then evacuated at the same temperature for 30 min. The reaction products were analyzed by gas chromatography. The column packings were 1.5 m of Porapak T at 413 K for separation of CO_2, HCHO, CH_3OCH_3, H_2O, CH_3OH, $HCOOCH_3$, and $(CH_3O)_2$ CH_2 and 3 m of Porapak T at 213 K for separation of O_2 and CO. The catalytic activity (TON) was calculated from the initial rate of methanol consumption per Mo atom.

RESULTS AND DISCUSSION

The Effect of the pH of the Impregnating Solution

The ^{95}Mo NMR spectra of the impregnating solution at different pH values are shown in Fig. 1. In the basic solutions (pH > 7.61), only the sharp resonance line of tetrahedrally coordinated Mo species (MoO_4^{2-}) is observed at −1.75 ppm. In the acidic solutions region (pH < 5.26), a broad resonance peak is observed at 33.3 ppm; this is attributed to octahedrally coordinated Mo species (presumably $Mo_7O_{24}^{6-}$) (*17*). At the intermediate pH regions (6.45 > pH > 5.42), both tetrahedral and octahedral Mo species are observed in the spectra, and the relative intensities of each peak vary as a function of pH.

The UV spectra of the impregnating solutions were measured after the samples were equilibrated (ca. 100 h) at different pH values. Typical spectra are shown in Fig. 2. The spectra of the acidic solutions differ from those of the basic solutions. At acidic pH values (D, E, and F in Fig. 2), two characteristic bands were observed at about 260

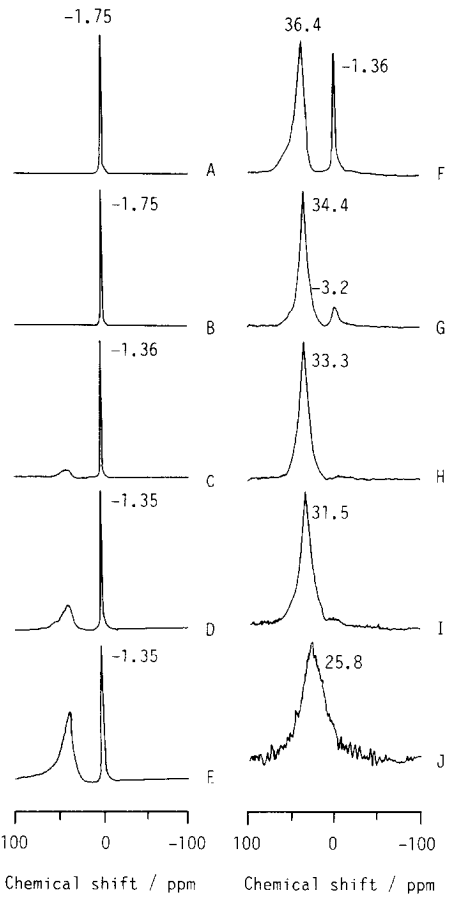

FIG. 1. ^{95}Mo NMR spectra of 0.1 *M* Mo solution at different pH values: (A) pH 9.31, (B) pH 7.61, (C) pH 6.45, (D) pH 6.10, (E) pH 5.86, (F) pH 5.73, (G) pH 5.42, (H) pH 5.26, (I) pH 4.64, (J) pH 3.43.

and 315 nm. The band at 260 nm is attributed to the charge transfer band of Mo^{6+}=O^{2-} (*18*), and the band at 315 nm is that of bridged Mo–O–Mo (*19*). However, as the pH values increased, the 315-nm band decreased in intensity, and at basic pH values (A and B in Fig. 2) only the 260-nm band remained.

The NMR and UV spectroscopic studies suggest that polymeric species, $Mo_7O_{24}^{6-}$ or $Mo_8O_{26}^{4-}$, are present in the acidic pH regions (pH < 5.26), and that monomeric species, MoO_4^{2-}, in the basic pH regions (pH > 7.61) were preferentially adsorbed on the titania surface during impregnation.

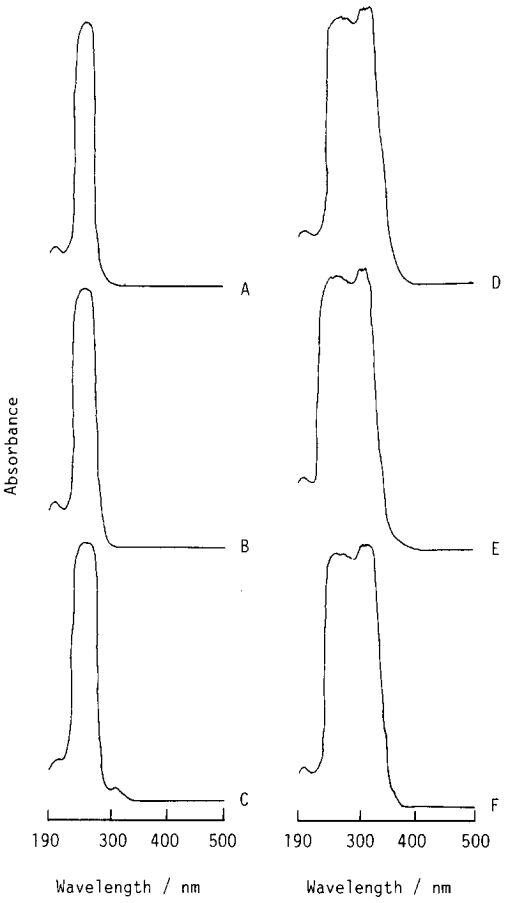

FIG. 2. UV spectra of impregnating solutions of molybdate anion after equilibrium adsorption for 100 h: (A) pH 9.69, (B) pH 7.28, (C) pH 6.47, (D) pH 5.26, (E) pH 3.98, (F) pH 2.86.

Surface Properties of Calcined Catalysts

The effect of pH on the surface properties of MoO_3/TiO_2 catalysts is shown in Table 1. The initial pH value of the impregnating solution tends to shift toward IEP of the titania in order to compensate for the net charge of the titania surface. Segawa and Hall (*20*) previously showed that CO_2 chemisorbs selectively on the hydroxyls of the Al_2O_3 support surface but does not show any chemical interaction with surface molybdena species; similar behavior (*21*) was found for the MoO_3/TiO_2 catalysts. The amounts of chemisorbed CO_2 are affected by the Mo loadings on TiO_2, decrease concomitantly as the adsorbed amounts of molybdate anion increase, and approach zero at about 6.6 wt% (pH 3.98). This result shows that the hydroxyls of titania were replaced by the molybdate anion as a function of Mo loadings so that at about 6.6 wt% almost all the hydroxyls were bound to molybdena species. The surface area value at lower Mo loading (below 4.2 wt%) remained unchanged, but at higher loading it decreased slightly. However, the surface area per gram of titania instead of per gram of catalyst was constant regardless of Mo loading up to 6.6 wt%. This result indicates that the catalysts dispersed homogeneously on the titania surface up to 6.6 wt% reaching the monolayer coverage of MoO_3 on TiO_2 and is directly supported by the XPS and Raman data which will be described in the next section.

Figure 3 shows the relation between the final pH values of impregnating solution and Mo loadings of catalysts after calcination at 773 K. The adsorbed amounts of molybdate anions were strongly dependent on the final pH of molybdic solution and they increased as the pH values decreased. Furthermore, they drastically changed near IEP of titania (pH 6.2) and IEP of Mo^{6+} (pH 1.5) (*13*). The sharp decreasing of Mo loading near IEP of titania was due to the electrostatic repulsion between the molybdate anion and the larger population of negatively charged surface titania. The cause of the secondary increasing near IEP of Mo^{6+} at pH 1.5 is not clear. Wang and Hall (*9*) suggested that different exposed crystal planes of the support have different exposed IEP or that higher polymeric molybdate species formed on the support surface. The result of a blank test shows that precipitation occurred around pH 1.5, so that the formation of precipitation (*22, 23*) also leads to an increasing of the Mo loading.

XRD patterns of the MoO_3/TiO_2 catalysts after calcination at 773 K are shown in Fig. 4. The XRD patterns exhibit different phases as a function of Mo loading. Up to 6.6 wt% MoO_3/TiO_2, only the diffraction

TABLE 1

Surface Properties of MoO_3/TiO_2 Catalysts Prepared by an Equilibrium Adsorption Method

Mo loading/ wt%	Initial[a] pH	Final[a] pH	CO_2 chemisorption		Surface area ($m^2\ g^{-1}$)
			CO_2 uptake/ mol g^{-1}	% of free titania	
0.0	—	—	145.0	100.0	51.0 (51.0)[b]
2.4	9.77	9.69	97.5	68.2	49.4 (50.6)
3.5	8.81	8.68	67.4	46.5	49.5 (51.1)
4.2	7.86	7.28	47.6	32.8	49.2 (51.4)
6.4	5.06	5.72	10.3	7.1	46.4 (49.6)
6.6	3.91	3.98	5.8	4.0	46.4 (49.7)
7.1	2.53	2.61	0.0	0.0	42.2 (45.4)
20.0	0.99	1.24	0.0	0.0	34.4 (43.0)

[a] Initial and final pH values in impregnating solution.
[b] Numbers in parentheses represent surface areas per gram of titania.

lines attributed to the titania support were observed. Crystalline MoO_3 was only detected in the 20 wt% catalyst (A in Fig. 4). The absence of crystalline MoO_3 phase in the XRD pattern up to 6.6 wt% catalysts suggests that for these catalysts the molybdena species are present in either an amorphous state or as small crystallites of less than 4 nm in diameter which are undetectable by XRD.

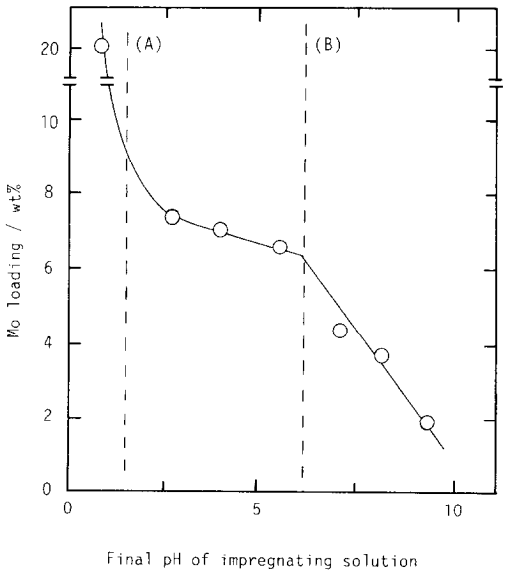

FIG. 3. Relation between Mo loadings and pH of the impregnating solution: (A) IEP of Mo^{6+} (pH 1.5); (B) IEP of TiO_2 (pH 6.2).

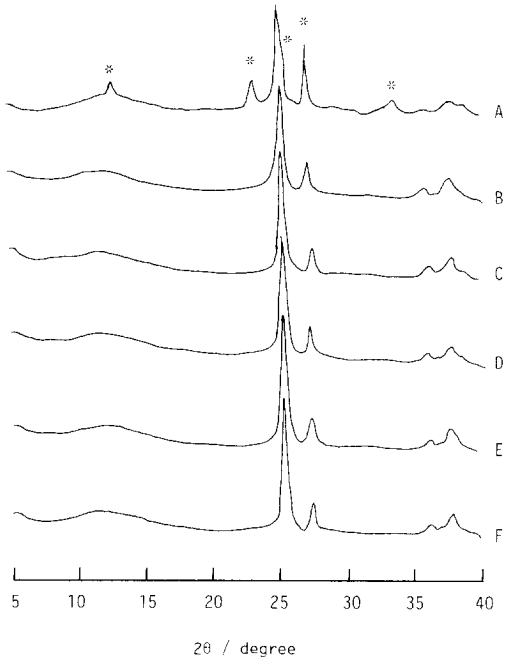

FIG. 4. XRD patterns of MoO_3/TiO_2 catalysts as a function of Mo loadings: (A) 20.0 wt% (pH 1.24), (B) 6.6 wt% (pH 3.98), (C) 4.2 wt% (pH 7.28), (D) 3.5 wt% (pH 8.68), (E) 2.4 wt% (pH 9.69), (F) TiO_2 support. (*) Represents the crystalline MoO_3.

The laser Raman spectra of the calcined catalysts were obtained under ambient conditions and are presented in Figs. 5 and 6. The titania support exhibits strong Raman bands at 395, 516, and 637 cm^{-1} and weak Raman bands at 446 and 790 cm^{-1} (B–E in Fig. 5). The strong bands at 395, 516, and 637 cm^{-1} originate from the TiO_2 (anatase) phase and the weak band at 446 cm^{-1} is due to the TiO_2 (rutile) phase (*24*). The weak band at 790 cm^{-1} is due to the first overtone of the 395 cm^{-1} band of anatase. The Raman spectrum of the titania support is dominated by the features of TiO_2 (anatase) because the Raman scattering cross section of the anatase phase is much higher than that of the rutile phase. The titania support does not possess any Raman bands between 800 to 1050 cm^{-1}. The adsorption of molybdenum oxide on titania introduced a new Raman feature in the 940–970-cm^{-1} range for the 2.4- to 7.1-wt% MoO_3/TiO_2 catalysts. This new band has previously been shown to originate from a two-dimensional molybdenum oxide overlayer on the titania support surface (*11, 25, 26*). The intensity of the Raman band of surface molybdenum oxide is increased with Mo loading. The 7.1-wt% MoO_3/TiO_2 catalyst also exhibits a

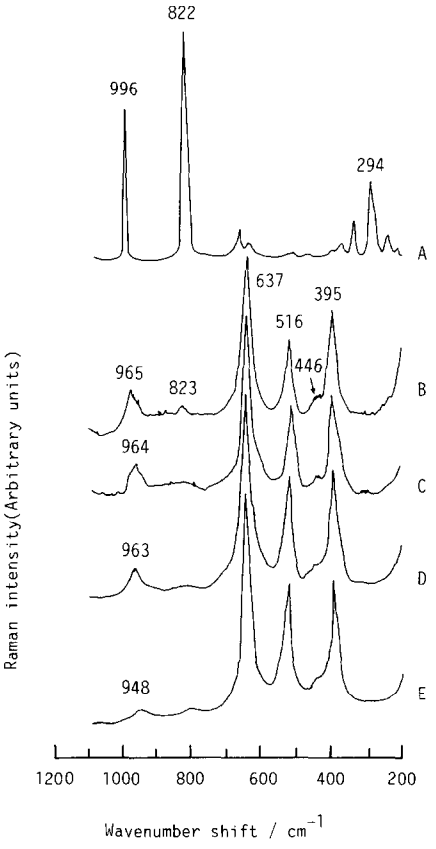

FIG. 5. Laser Raman spectra of MoO_3/TiO_2 catalysts as a function of Mo loadings: (A) 20 wt% (pH 1.24), (B) 7.1 wt% (pH 2.61), (C) 6.4 wt% (pH 5.72), (D) 4.2 wt% (pH 7.28), (E) 2.4 wt% (pH 9.69).

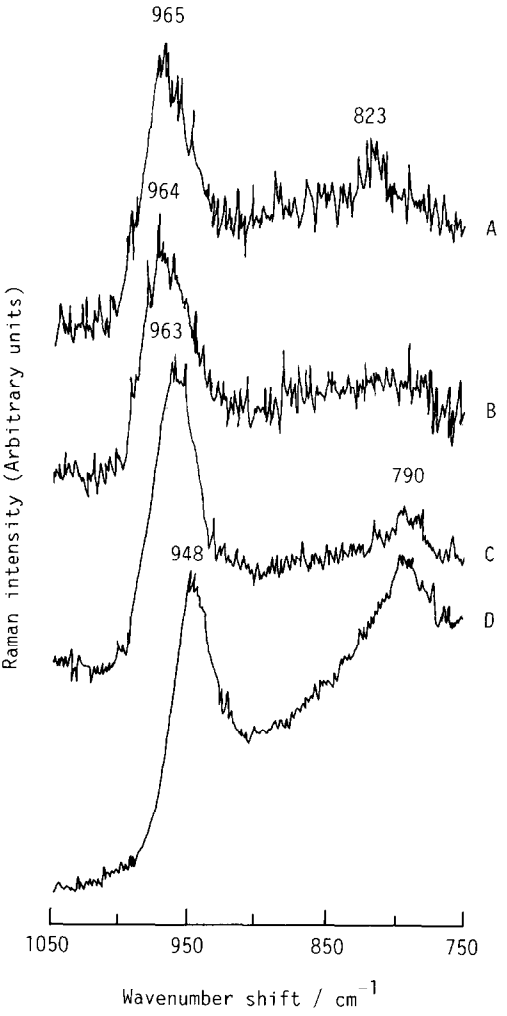

FIG. 6. Laser Raman spectra of MoO_3/TiO_2 catalysts as a function of Mo loadings: (A) 7.1 wt% (pH 2.61), (B) 6.6 wt% (pH 3.98), (C) 4.2 wt% (pH 7.28), (D) 2.4 wt% (pH 9.69). The bands at 823 and 790 cm^{-1} are crystalline MoO_3 and the first overtone of the 395 cm^{-1} (anatase), respectively.

very weak Raman band at 823 cm^{-1}, which is characteristic of crystalline MoO_3 particles. Thus, the 7.1-wt% MoO_3/TiO_2 catalyst possesses a molybdenum oxide coverage slightly in excess of monolayer, and about 6.6 wt% of MoO_3/TiO_2 corresponds to a monolayer of surface molybdenum oxide on the titania support possessing 51 m^2 g^{-1} (see Fig. 6). This result is in excellent agreement with previous Raman studies of the MoO_3/TiO_2 system (*11, 25, 26*). The 20 wt% MoO_3/TiO_2 catalyst (A in Fig. 5) exhibits very strong Raman bands at 996 and 822 cm^{-1}, as well as additional bands at ca. 294 cm^{-1}, which are due to the presence of crystalline MoO_3 (*25, 26*). The very strong Raman scattering from the crystalline MoO_3 particles dominates the Raman spectrum at high crystalline MoO_3 contents.

The structure of the surface molybdenum oxide species on the titania support can be determined from comparison of the Raman vibrational data of the MoO_3/TiO_2 catalysts and reference molybdenum oxide compounds. The Raman active Mo–O stretching vibrations of tetrahedral and octahedral molybdenum oxide reference compounds are tabulated in Table 2. The isolated MoO_4^{2-}(aq) ion (Raman band at 897 cm^{-1}) possesses an ideal tetrahedral structure.

TABLE 2

Raman Mo–O (Terminal) Stretching Frequencies of Molybdate Reference Compounds

Tetrahedral molybdate compounds	
$CaMoO_4$	880 cm^{-1}
MoO_4^{2-}(aq)	897 cm^{-1}
$(NH_4)_2Mo_2O_7$	910 cm^{-1}
$K_2Mo_2O_7KBr$	928 cm^{-1}
Octahedral molybdate compounds	
Ba_2CaMoO_6	812 cm^{-1}
γ-Bi_2MoO_6	853 cm^{-1}
$(NH_4)_6Mo_7O_{24}4H_2O$	934 cm^{-1}
$Mo_7O_{24}^{6-}$(aq)	940 cm^{-1}
$Mo_8O_{26}^{4-}$(aq)	961 cm^{-1}
$(NH_4)_4Mo_8O_{26}5H_2O$	963 cm^{-1}
MoO_3	997 cm^{-1}

Crystalline $CaMoO_4$ possesses a scheelite structure where the isolated MoO_4 groups (Raman band at 880 cm^{-1}) is slightly distorted from the regular tetrahedral symmetry of the MoO_4^{2-}(aq) ion and assumes S_4 site symmetry (*27, 28*). Isolated, dimeric MoO_3–O–MoO_3 (Raman band at 928 cm^{-1}) is present in the molten salt $K_2Mo_2O_7KBr$ (*29*). Higher oligomers of molybdena tetrahedra are not known to exist (*30*). A slightly distorted MoO_4 species (Raman band at 910 cm^{-1}) exists in $(NH_4)_2Mo_2O_7$ as part of a linear polymer composed of alternating molybdena octahedra and tetrahedra (*31*). An ideal MoO_6 octahedron would be expected to exhibit a stretching mode at ca. 700 cm^{-1} (by analogy to Li_6WO_6 (*32*)). Compounds containing the MoO_6 octahedron are usually slightly distorted and exhibit the stretching mode at $\geq$800 cm^{-1} (*33, 34*). A somewhat greater degree of distortion is present in the MoO_6 octahedron found in γ-Bi_2MoO_6, where the Mo–O stretching mode of highest frequency occurs at 853 cm^{-1} (*35*). The majority of molybdena octahedra possess a highly distorted MoO_6 group containing one very short Mo–O bond (<0.18 nm) and one very long Mo–O bond (>0.23 nm) with a molecular geometry resembling the distorted square pyramid; stretching frequencies for the short Mo–O bond are in the 940–1000-cm^{-1} range. Such highly distorted MoO_6 octahedra are found in $(NH_4)_6Mo_7O_{24}4H_2O$ (*36*) (Raman band at 934 cm^{-1}), $Mo_7O_{24}^{6-}$(aq) (Raman band at 940 cm^{-1} (*37*)), $(NH_4)_4Mo_8O_{26}5H_2O$ (*38*) (Raman band at 963 cm^{-1}), $Mo_8O_{26}^{4-}$(aq) (Raman band at 961 cm^{-1} (*37*)), and crystalline MoO_3 (Raman band at 997 cm^{-1}). The above information regarding the Mo–O stretching vibrations for the molybdena reference compounds are used to identify molybdate functionalities and to aid in the determination of the molybdate species present on the titania support.

The Raman spectra of the calcined MoO_3/TiO_2 catalysts exhibit bands in the 948- to 965-cm^{-1} region (see Figs. 5 and 6).

The position of the Mo–O stretch for MoO_3/TiO_2 is much higher than that for the ideal tetrahedral structure of MoO_4^{2-}(aq) (897 cm^{-1}) or the distorted tetrahedral structures of $(NH_4)_2Mo_2O_7$ (910 cm^{-1}) and $K_2Mo_2O_7KBr$ (928 cm^{-1}). The position of the band for MoO_3/TiO_2 is also much higher than that of the slightly distorted MoO_6 octahedra of Ba_2CaMoO_6 (812 cm^{-1}) and of γ-Bi_2MoO_6 (853 cm^{-1}). The position of the Raman bands for MoO_3/TiO_2, however, falls in the region observed for highly distorted MoO_6 octahedra. Thus, it appears that the surface molybdenum oxide species on TiO_2 possess a highly distorted MoO_6 structure (distorted square pyramidal). The slight shift in the Raman band position with molybdenum oxide loading is most likely related to additional distortions caused by interactions among the surface molybdenum oxide species at the higher surface coverages. The strong titania Raman bands below 700 cm^{-1} interfere with the detection of diagnostic Raman bands for other molybdate functionalities; the bending mode of the Mo–O–Mo linkage is found in the 200- to 300-cm^{-1} region of the spectrum.

The XPS Mo(3*d*)/Ti(2*p*) peak area intensity ratios as a function of Mo loading for the calcined catalysts are shown in Fig. 7. The Mo(3*d*)/Ti(2*p*) ratios increase linearly up to ca. 6.6 wt% and then level off from the linear relationship for further increases of Mo loadings. The result indicates that the molybdena species adsorbed homogeneously on the titania surface and reached monolayer coverage at about 6.6 wt%; such a result agrees with the Raman observations. Beyond the monolayer coverage, the molybdena species are adsorbed on the titania surfaces with multilayer form (crystalline MoO_3).

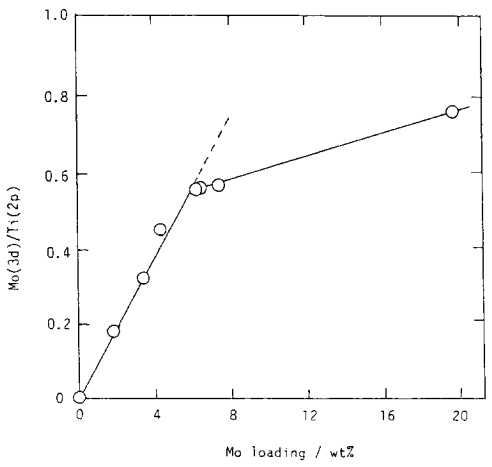

FIG. 7. XPS Mo(3*d*)/Ti(2*p*) ratio as a function of Mo loadings.

Catalytic Reaction

The catalytic activities and selectivities of methanol oxidation as a function of the Mo loadings are presented in Table 3. The titania support itself is inert for the methanol oxidation at 473 K. High catalytic activities up to monolayer coverage (6.6 wt%) were observed regardless of Mo loading. However, above monolayer coverage, the activities decreased as the Mo loading increased. The decrease in catalytic activity above monolayer is due to the increase of MoO_3 crystallites which are less active than surface molybdate species. The catalysts prepared by an equilibrium adsorption method showed slightly higher catalytic activities than those of the catalysts prepared by the standard impregnation method. The higher catalytic activities reflect the higher dispersion and greater homogeneity of catalysts. The selectivity of CH_3OCH_3, which cannot be formed via oxidative dehydrogenation, increased as the Mo loadings increased. The formation of CH_3OCH_3 may be facilitated by the acidic sites of catalyst surfaces. Segawa and Hall (*39*) have reported that both Lewis-bounded pyridine (LPy) and pyridium ion (BPy) occur on the oxide form of molybdena–alumina catalysts. The catalyst prepared at high pH regions showed no Brønsted acidity, but Brønsted acidity increased linearly when Mo loading increased. Kataoka and Dumesic (*40*) have also found that, although no Brønsted acidic sites were observed on 1 wt% Mo/SiO_2 under water-free conditions, small numbers of Brønsted acidic sites

TABLE 3

Catalytic Activity and Selectivity for Methanol Oxidation on MoO_3/TiO_2 Catalysts

Mo loading/ wt%	pH[a]	Reaction rate[b]/ 10^{-2} s^{-1}	Selectivity[c]			
			CH_3OCH_3	HCHO	$HCOOCH_3$	$(CH_3O)_2CH_2$
2.4	9.69	2.75 (1.92)[d]	0.00	4.25	32.16	63.59
3.5	8.69	2.67	0.65	5.07	33.36	60.87
4.2	7.28	2.71 (2.39)	3.50	4.50	33.50	58.50
6.6	3.98	2.89 (2.32)	6.81	4.70	28.95	59.50
6.6[e]	3.98	11.80	7.50	15.50	25.00	52.00
7.7	2.86	2.34 (1.82)	11.70	5.60	28.70	54.00
20.0	1.24	0.41 (0.65)	19.40	3.70	25.80	51.10

[a] Final pH value of impregnating solution.
[b] Initial rate of methanol consumption at 473 K.
[c] Selectivity of each product at 25 mol% conversion of methanol.
[d] Numbers in parentheses are reaction rate on MoO_3/TiO_2 catalysts prepared by standard impregnation method.
[e] Reaction at 513 K.

were detected for the 6.4 wt% Mo/SiO_2 sample. The origin of acidic sites on the MoO_3/TiO_2 catalysts is the acidic hydroxyl groups which are thought to be generated on the surface of the catalyst by the hydration of polymeric Mo cluster.

The selectivity of each product of methanol oxidation over 6.6-wt% catalyst as a function of the conversion is shown in Fig. 8. At low conversions the main product was $(CH_3O)_2CH_2$, but at high conversions mostly $HCOOCH_3$ was formed. Only trace amounts of CO and CO_2 were formed over the whole range of the reaction. The low selectivity for HCHO is observed regardless of Mo loadings. This result suggests that the formation of HCHO is less likely than that of $(CH_3O)_2CH_2$ at the lower reaction temperature used in this investigation. The selectivity for the HCHO increased with increasing reaction temperature (see Table 3).

When $(CH_3O)_2CH_2$ was used as the reactant for oxidation (6.6 wt%, pH 3.98) as shown in Fig. 9, the oxidation products were $HCOOCH_3$, CH_3OCH_3, HCHO, and CH_3OH, and the major product was $HCOOCH_3$ under separate experiments. The oxidation of CH_3OCH_3 and the oxidation of $HCOOCH_3$ were also examined. Neither reaction showed any catalytic activity over the MoO_3/TiO_2 catalysts.

The reaction pathway of methanol oxida-

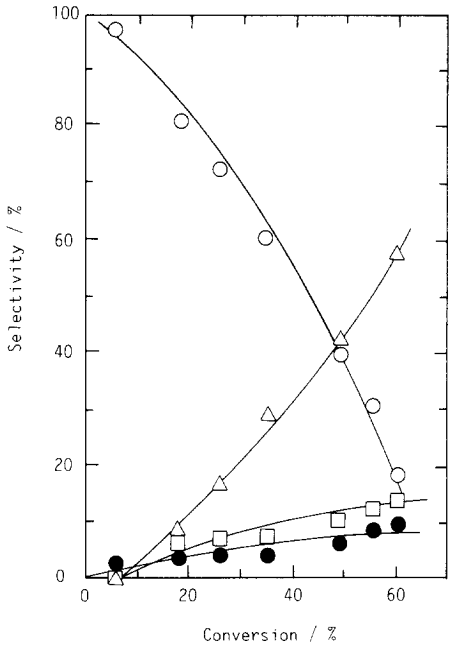

FIG. 8. Selectivity of reaction products as a function of the conversion of methanol oxidation over MoO_3/TiO_2 catalyst (6.6 wt%, pH 3.98): (○) $(CH_3O)_2CH_2$; (●) HCHO; (□) CH_3OCH_3; (△) $HCOOCH_3$.

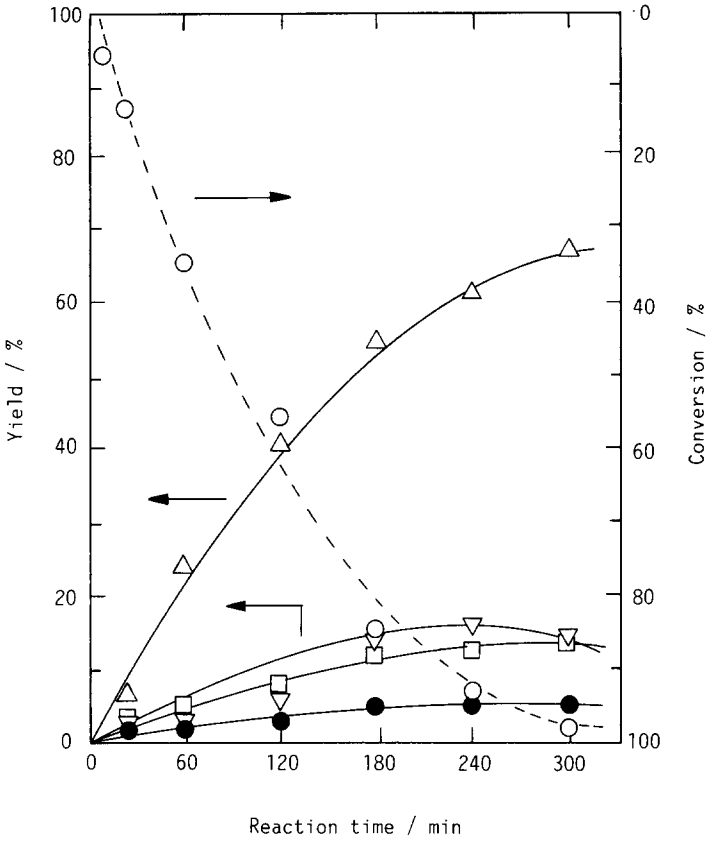

FIG. 9. $(CH_3O)_2CH_2$ oxidation over MoO_3/TiO_2 catalyst (6.6 wt%, pH 3.98): (○) $(CH_3O)_2CH_2$; (▽) CH_3OH; (●) HCHO; (□) CH_3OCH_3; (△) $HCOOCH_3$.

tion previously proposed for the V_2O_5 system (*41*) is shown in Scheme 1. Dissociative adsorption of methanol produces methoxy intermediates which react with neighboring methoxy groups or physically adsorbed methanol to produce CH_3OCH_3. On the other hand, abstraction of H-atom from the methoxy group by an adjacent oxygen can result in the formation of oxymethylene intermediates. Either desorption or condensation of oxymethylene intermediates may produce gaseous HCHO and/or $(CH_3O)_2CH_2$. Desorption of oxymethylene is much slower than the condensation. Thus oxymethylene intermediates react readily with gaseous methanol to give $(CH_3O)_2CH_2$ preferentially at low conversion regions (see Fig. 8). In addition, further oxidation of oxymethylene produces adsorbed formate intermediates via dioxymethylene intermediates; these react with methoxy groups to give $HCOOCH_3$. The decomposition of $(CH_3O)_2CH_2$ also forms $HCOOCH_3$ irreversibly. In summary, the catalytic active sites of methanol oxidation are proposed to be double-bond oxygens (Mo=O) on surface molybdate species. The selectivity of CH_3OCH_3, which is produced by acidic sites on the molybdena/titania surface, increases as Mo loading increases.

CONCLUSIONS

The colloidal chemistry of the impregnating solutions allows us to explain the genesis of the molybdena/titania catalysts. At acidic pH regions, octahedral molybdate anions, $Mo_7O_{24}^{6-}$, are present in solution; at

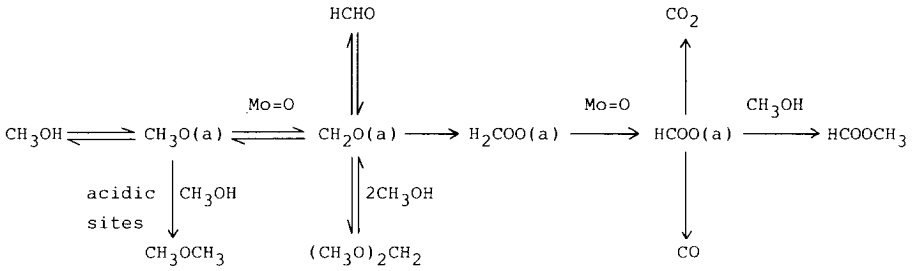

SCHEME 1. Reaction pathway of methanol oxidation on MoO_3/TiO_2 catalysts.

basic pH regions, tetrahedrally coordinated molybdate anions, MoO_4^{2-}, are present.

For the calcined catalysts, XPS and Raman spectroscopic studies show that monolayer coverage of the surface molybdenum oxide species is established at about 6.6 wt% (pH 3.98). Up to monolayer coverage, the molybdena species are highly dispersed on the titania surface. The Raman studies show that the surface molybdenum oxide species possess a highly distorted MoO_6 octahedral structure with one short Mo=O bond. The structure of the surface molybdena species, distorted MoO_6 octahedral, is found to be independent of the starting solution pH ($2.86 \leq pH \leq 9.69$). Further increase of molybdena loading above monolayer coverage results in the formation of a crystalline MoO_3 phase.

The methanol oxidation studies indicate that the turnover numbers and selectivity are strongly dependent on the structure and dispersion of the surface molybdate species in the MoO_3/TiO_2 catalysts. The catalysts up to monolayer coverage show higher turnover numbers than the catalysts exceeding monolayer coverage (i.e., possessing crystalline MoO_3). A high selectivity for oxidation products [$(CH_3O)_2CH_2$, $HCOOCH_3$, and HCHO] is observed on the catalysts containing low molybdena loadings. The selectivity toward the dehydration product CH_3OCH_3, which is facilitated by acidic sites, increases with molybdena loading.

REFERENCES

1. Yang, T. J., and Lunsford, J. H., *J. Catal.* **103,** 55 (1987).
2. Iwasawa, Y., and Yamagishi, M., *J. Catal.* **82,** 373 (1983).
3. Allison, J. N., and Goddard, W. A., III, *J. Catal.* **92,** 127 (1985).
4. Louis, C., Tatibouet, J. M., and Che, M., *J. Catal.* **109,** 354 (1988).
5. Giordano, N., Castellan, A., Bart, J. C. J., Vaghi, A., and Campadelli, F., *J. Catal.* **37,** 204 (1975).
6. Sonnemans, J., and Mars, P., *J. Catal.* **31,** 209 (1973).
7. Hall, W. K., and Massoth, F. E., *J. Catal.* **34,** 41 (1974).
8. Weigold, H., *J. Catal.* **83,** 85 (1983).
9. Wang, L., and Hall, W. K., *J. Catal.* **77,** 232 (1982).
10. Brunelle, J. P., *Pure Appl. Chem.* **50,** 1211 (1978).
11. Ng, K. Y. S., and Gulari, E., *J. Catal.* **92,** 340 (1985).
12. Haight, G. P., and Boston, D. R., *in* "Proceedings, 1st Inter. Climax Conf. on the Chemistry and Uses of Molybdenum" (P. C. H. Mitchell, Ed.), p. 48. London, 1973.
13. Parks, G. A., *Chem. Rev.* **65,** 177 (1965).
14. Parfitt, G. D., *Pure Appl. Chem.* **48,** 415 (1976).
15. D'Aniello, M. J., Jr., *J. Catal.* **69,** 9 (1981).
16. Lundell, G. E. F., and Bright, H. A., *in* "Applied Inorganic Analysis," 2nd ed., p. 303. Wiley, New York, 1953.
17. Luthra, N. P., and Cheng, W. C., *J. Catal.* **107,** 154 (1987).
18. Jeziorowski, H., and Knozinger, H., *J. Phys. Chem.* **82,** 1166 (1979).
19. Rodrigo, L., Marcinkowska, K., Lafrance, C. P., Roberge, P. C., and Kaliaguine, S., *in* "Proceedings, 9th Ibero-American Symp. Catal.," p. 675. Lisbon, 1984.
20. Segawa, K., and Hall, W. K., *J. Catal.* **77,** 221 (1982).
21. Segawa, K., Kim, D. S., Kurusu, Y., and Wachs, I. E., *in* "Proceedings, 9th International Congress on Catalysis, Calgary, 1988" (M. J. Phillips and M. Ternan, Eds.), p. 1960. Chem. Institute of Canada, Ottawa, 1988.
22. Mulcahy, F. M., Haulla, M., and Hercules, D. M., *J. Catal.* **106,** 210 (1987).

23. Van Veen, J. A. R., De Wit, H., Emeis, C. A., and Hendriks, P. A. J. M., *J. Catal.* **107,** 579 (1987).
24. Chan, S. S., Wachs, I. E., Murrell, L. L., Wang, L., and Hall, W. K., *J. Phys. Chem.* **88,** 5831 (1981).
25. Lin, Y. C., Griffin, G. L., Chan, S. S., and Wachs, I. E., *J. Catal.* **94,** 108 (1985).
26. Quincy, R. B., Houalla, M., and Hercules, D. M., *J. Catal.* **106,** 85 (1987).
27. Nakamoto, N., *in* "Infrared and Raman Spectra of Inorganic and Coordination Compounds," 3rd ed. Wiley, New York, 1978.
28. Russell, J. P., and Loudon, R., *Proc. Phys. Soc.* **85,** 1029 (1965).
29. Becher, H. J., Brockmeyer, H. J., and Prigge, U., *J. Chem. Res.* **M,** 1670 (1978).
30. Wells, A. F., *in* "Structural Inorganic Chemistry." Clarendon Press, Oxford, 1984.
31. Armour, A. W., Drew, M. G. B., and Mitchell, P. C. H., *J. Chem. Soc. Dalton Trans.*, 1493 (1975).
32. Hauck, J., and Fadini, A., *Z. Naturforsch. B* **25,** 422 (1970).
33. Corsmit, A. F., Hoefdraad, H. E., and Blasse, G., *J. Inorg. Nucl. Chem.* **34,** 3401 (1972).
34. Blasse, G., and Corsmit, A. F., *J. Solid State Chem.* **6,** 513 (1973).
35. Hardcastle, F. D., Wachs, I. E., Buttrey, D. J., Jefferson, D. A., and Thomas, J. M., to be published.
36. Lindqvist, I., *Ark. Kemi* **2,** 325 (1951).
37. Aveston, J., Anacker, E. W., and Johnson, J. S., *Inorg. Chem.* **3,** 735 (1964).
38. Lindqvist, I., *Ark. Kemi* **2,** 349 (1951).
39. Segawa, K., and Hall, W. K., *J. Catal.* **76,** 133 (1982).
40. Kataoka, T., and Dumesic, J. A., *J. Catal.* **112,** 66 (1988).
41. Tronconi, E., Elmi, A. S., Ferlazzo, N., and Forzatti, P., *Ind. Eng. Chem. Res.* **26,** 1269 (1987).